



# Thermomechanical behavior and microstructural evolution in nodes and struts of face-centered cubic lattice structures during laser powder bed fusion processing

Muhammad Raihan Hashmi<sup>a,b</sup>, Soung Yeoul Ahn<sup>a,b</sup>, Gitaek Lee<sup>a,c</sup>, Jae-il Jang<sup>a,d</sup>, Zhe Gao<sup>d</sup>, Renhao Wu<sup>a,e,\*</sup>, Hyoung Seop Kim<sup>a,b,c,e,f,\*</sup>

<sup>a</sup> Center for Heterogenic Metal Additive Manufacturing, Pohang University of Science and Technology (POSTECH), Pohang 37673, Republic of Korea

<sup>b</sup> Department of Materials Science and Engineering, Pohang University of Science and Technology (POSTECH), Pohang, Republic of Korea

<sup>c</sup> School of Convergence Science and Technology, Pohang University of Science and Technology (POSTECH), Pohang 37673, Republic of Korea

<sup>d</sup> Division of Materials Science and Engineering, Hanyang University, Seoul 04763, Republic of Korea

<sup>e</sup> Graduate Institute of Ferrous and Eco-Materials Technology (GIFT), Pohang University of Science and Technology (POSTECH), Pohang 37673, Republic of Korea

<sup>f</sup> Advanced Institute for Materials Research (WPI-AIMR), Tohoku University, Sendai 980-8577, Japan

## ARTICLE INFO

### Keywords:

Laser powder bed fusion  
Lattice structures  
Finite element analysis  
Thermal history  
Microstructural heterogeneity

## ABSTRACT

Superior mechanical and functional properties, such as strength, ductility, and energy absorption capabilities, have garnered significant research interest in lattice structures, driven by advancements in additive manufacturing technologies. However, existing limitations in understanding the local thermal histories at the nodes and struts of lattice structures remain a topic to be explored. This study investigates the local thermal histories in lattice structures, focusing on variations in local microstructures. Numerical simulations, combined with detailed microstructure characterizations, reveal that nodes play a crucial role in determining the thermal history of lattice structures. The nodes and struts exhibit difference in grain size, porosity fractions and distortion due to heat dissipation. Furthermore, nodes and struts experience distinct thermal histories due to thermal cycling effects, resulting in microstructure heterogeneity.

## 1. Introduction

The development of additive manufacturing has enabled the fabrication of complex geometries that would have been otherwise difficult to manufacture using formative or subtractive methods. One geometry that has gained attention in recent years is the lattice structure. Also referred to as lightweight metallic lattice structures or metallic foams [1], they have demonstrated superior properties, serving as prosthetics in sophisticated biomedical applications [2,3] as well as in structural or functional applications such as vibration isolation [4] and energy harvesting [5]. The fabrication of lattice structures through additive manufacturing is thus of great importance, as these two important technologies complement each other, enabling the production of components tailored for specific applications [6,7].

The advantages of lattice structures are noteworthy, and studies have been conducted on their design [8,9], fabrication [10], mechanical

testing [11,12], and advanced characterization [13]. These structures exhibit complex geometries, which necessitate optimization of machine settings and parameters to achieve desired microstructures [14]. Computer-Aided Design (CAD) is thus employed to efficiently explore the design space [15] and assess the effects of processing parameters, which play a critical role in addressing issues such as porosity, microstructure evolution, thermal profiles, and deformation during fabrication. Recent studies have addressed common challenges related to microstructure evolution [16], functional properties [17], weight reduction [18], and numerical simulations to perform thermal profiling of the overall structure [19–21]. Moreover, lattice structures have been designed with varying relative densities to assess their effects on deformation, while imperfections have been introduced to enhance strength at low relative densities [22].

Fabrication procedures have been developed for lattice structures, varying process parameters to note the effect on the resulting product

\* Corresponding authors at: Center for Heterogenic Metal Additive Manufacturing, Pohang University of Science and Technology (POSTECH), Pohang 37673, Republic of Korea.

E-mail addresses: [wurenhao@postech.ac.kr](mailto:wurenhao@postech.ac.kr) (R. Wu), [hskim@postech.ac.kr](mailto:hskim@postech.ac.kr) (H.S. Kim).

<https://doi.org/10.1016/j.jalcom.2025.178883>

Received 14 November 2024; Received in revised form 19 January 2025; Accepted 27 January 2025

Available online 27 January 2025

0925-8388/© 2025 Elsevier B.V. All rights are reserved, including those for text and data mining, AI training, and similar technologies.

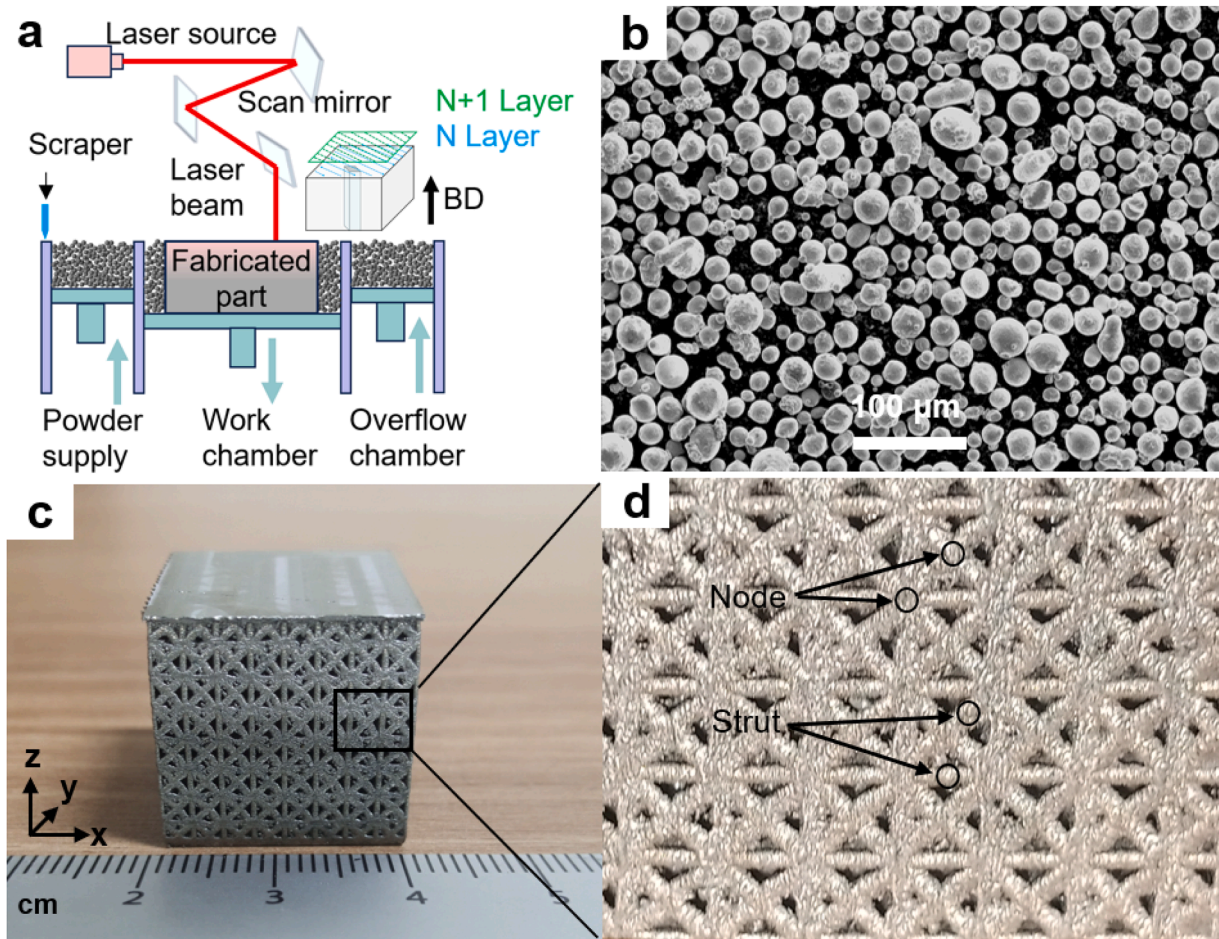


Fig. 1. (a) Schematic of the LPBF process, (b) powder morphology observed using SEM, (c) fabricated sample, and (d) enlarged view of the fabricated sample showing nodes and struts.

**Table 1**  
Dimensions of the FCC lattice structure.

Density (%)	10
Unit Cell Size (mm <sup>3</sup> )	2.5 × 2.5 × 2.5
Strut Diameter (mm)	0.25
Strut Thickness (mm)	0.42
Overall Dimensions of the Lattice Structure (mm <sup>3</sup> )	20 × 20 × 20

**Table 2**  
Process parameters used for the LPBF fabrication of the lattice structure.

Parameter	Value
Laser power (W)	370
Laser scanning speed (mm/s)	1300
Hatch spacing (mm)	0.08
Layer spot size (μm)	70
Laser thickness (μm)	50
Laser scan rotation angle (°)	67

[23,24], and simulation studies have been conducted to investigate thermal profiles and histories of additively manufactured parts. Moreover, studies inspired by natural phenomena have sought to replicate damage-resistant responses observed in natural lattice structures, applying them in fabrication [25]. Liu et al. [26] studied the microstructural response of lattice structures to thermal gradients. Research has also been done on architecture materials known as Archimats [27]

**Table 3**  
Process parameters in transient numerical thermal analysis.

Build Settings in Simulation	Value
Hatch spacing (mm)	0.08
Deposition thickness (μm)	0.04
Dwell time (s)	5
Preheat temperature (°C)	22
Gas convection coefficient (for both build and cooldown conditions) (W/mm <sup>2</sup> )	1 × 10 <sup>-5</sup>
Powder convection coefficient (for both build and cooldown conditions) (W/mm <sup>2</sup> )	1 × 10 <sup>-5</sup>

with mutually conforming geometries based on their interlocking design concept [28]. These studies have been done on lattice structures and have also explored the development of patterned microstructures through Severe Plastic Deformation (SPD), which result in ultra-fine-grained materials [29]. Building on this, Alaña et al. characterized the microstructure at the node and strut [30], but relied primarily on experimental methods. Numerical simulations have been employed to study the mechanical response of lattice structures [31]; however, determining thermal behavior during processing has been less explored. The Finite Element Method (FEM) simulations to predict thermal profile and histories, which can provide insight into microstructure prediction, represent an area with considerable potential for further exploration.

While studies have been performed on various aspects of lattice structures, limited work has been done to determine the thermal profiles and histories at the nodes and struts through numerical simulations, and

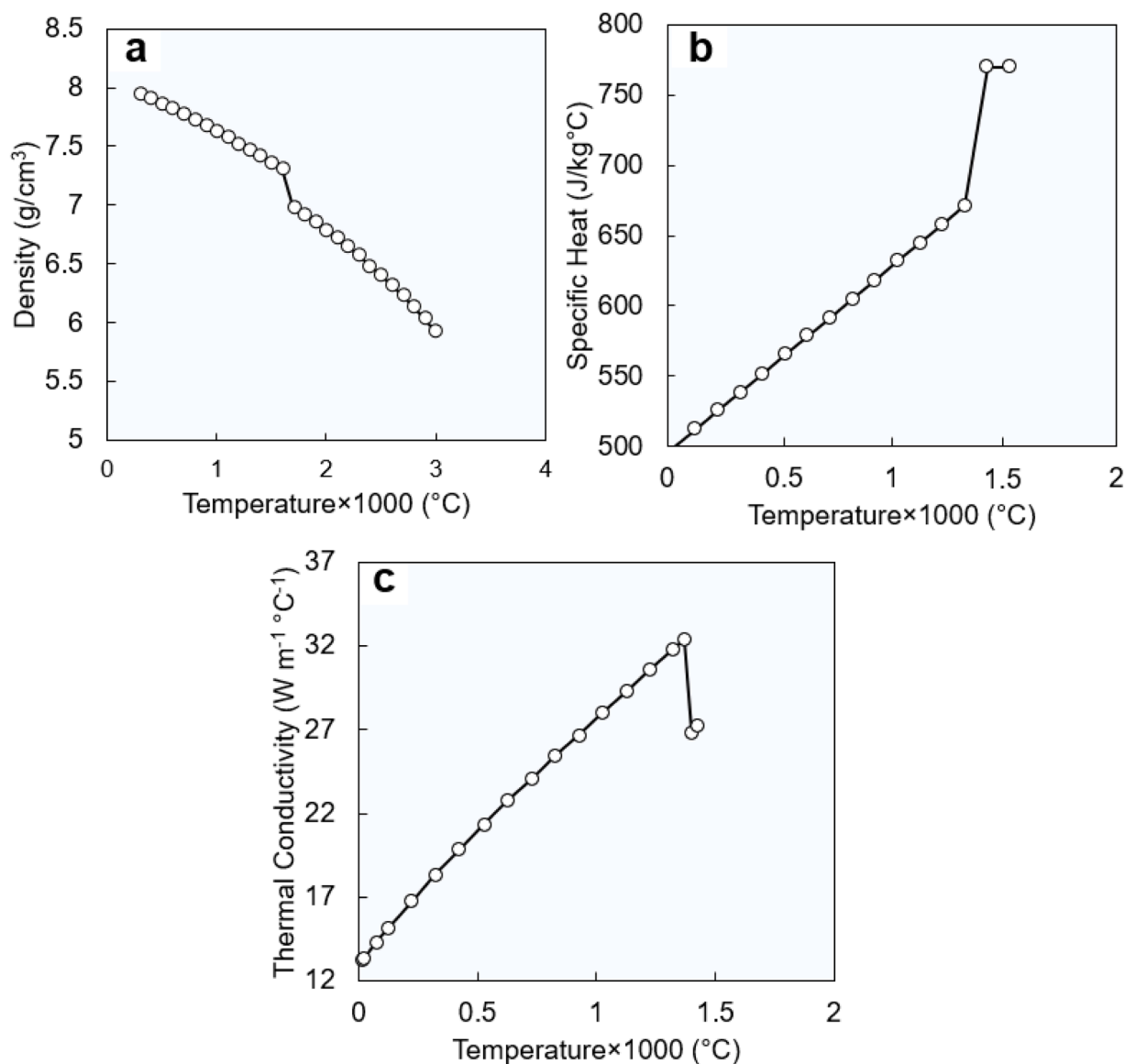


**Fig. 2.** Thermal properties used as material parameters in the transient thermal simulations to determine the thermal histories of the nodes and struts in the lattice structure with (a), (b) and (c) showing changes with temperature in density, specific heat, and thermal conductivity, respectively. (data of SS 316 L used from Ansys Workbench Engineering Data Version 2023 R1).

to validate these profiles and histories with microstructure studies. The goal of this study is to bridge this gap by performing numerical simulations to obtain the thermal history of lattice structures at the nodes and struts. The thermal histories predicted by numerical simulations, in conjunction with thermal cycling effects, will be validated through microstructural analysis such as grain size, pore fraction and distortion in the node and strut, to explore how microstructures at the nodes and struts are affected by distinct thermal histories as a function of distinct thermal dissipation. This study aims to ensure that the thermal behavior predicted by numerical simulations is reflected in the microstructure, providing a comprehensive understanding of the relationship between thermal history and microstructural evolution in lattice structures.

## 2. Materials and methods

### 2.1. Laser powder bed fusion process

The lattice structure was fabricated using Laser Powder Bed Fusion (LPBF) on a GE Additive Concept Laser M2 Series 5 machine. A

schematic of the LPBF process is given in Fig. 1(a). A face-centered cubic (FCC) lattice structure with dimensions of 20 mm in length, width, and height, and a relative density of 10 %, unit cell strut diameter 0.25 mm and strut thickness 0.42 mm was fabricated using gas-atomized austenitic 316 L stainless steel powder, purchased from GE Additive. The dimensions are summarized in Table 1. The average particle size was measured to be 30  $\mu\text{m}$  (Fig. 1b). To minimize the sample size effect [32], an  $8 \times 8 \times 8$  (XYZ direction unit cells) geometry was fabricated (Fig. 1c). Detailed processing parameters are provided in Table 2. The same fabrication methods were employed in our previous work [33], with different build parameters assigned to different regions of the lattice.

### 2.2. Microstructure and mechanical properties

After fabrication, the lattice structure was sectioned along the build direction and polished with diamond paste and colloidal solution for microscopic analysis. Electron backscatter diffraction (EBSD) analyses were performed to assess microstructural characteristics. The EBSD

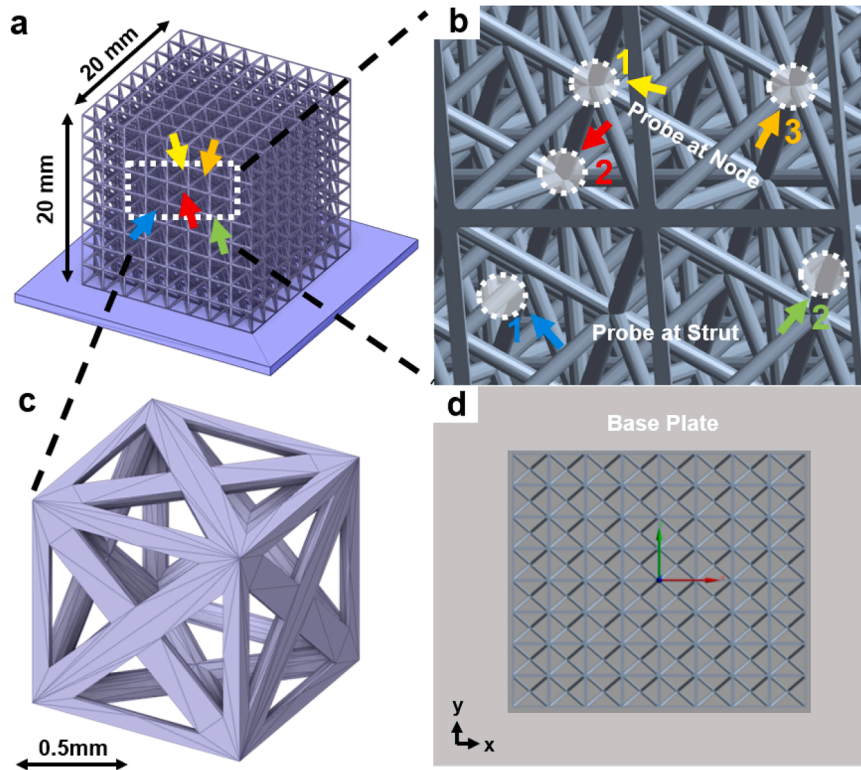


**Fig. 3.** (a) Isometric view of the lattice  $8 \times 8 \times 8$  FCC lattice structure, (b) schematic of the thermal probes placed at the nodes and struts, (c) unit cell of the lattice structure, and (d) top view ( $z$  plane out of the page) of the lattice structure showing the geometrical origin.

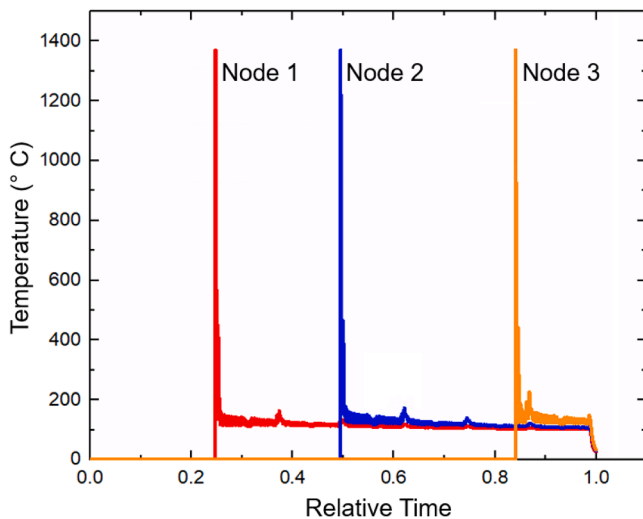


**Fig. 4.** Temperature of the nodes recorded by the thermal probes. The values in brackets represent the coordinates of the probes relative to the origin, as shown in Fig. 2. The small temperature spikes indicate that the fabrication of nodes connected to ten struts increases the temperature of the overall system.

equipment used was a Scanning Electron Microscope (Model Ultra-55), manufactured by ZEISS, with an accelerated voltage of 20 kV, working distance of 8 mm, and a step size of  $2.27 \mu\text{m}$ . Data obtained through the FE-SEM EBSD were processed using AZtecCrystal Processing Software, with further processing done on EDAX OIM software.

To compare mechanical properties of the nodes and struts, nanoindentation tests were performed at the nodes and struts separately using a Nanoindenter – XP G200 KLA. Twenty indentations were performed at both the node and struts. Nodes and struts were tested at 10

locations across the lattice structure, resulting in a total of 400 indentations on the specimen. The maximum pressure ( $P_{\text{max}}$ ) was 20 mN, with a strain rate of  $0.05 \text{ s}^{-1}$  used for the tests.

### 2.3. Finite element method simulations

The LPBF process simulation was conducted using ANSYS Workbench, utilizing the element birth and death method [34]. In this technique, all elements in the meshed geometry are initially inactive and are sequentially activated as the layers are deposited, mimicking the layer-by-layer nature of the LPBF process. The simulation model settings, shown in Table 3, were aligned with the experimental conditions to ensure a close approximation of the thermal behavior observed during actual fabrication.

For heat transfer analyses, explicit FEM was used. Mesh size for the FEM model was carefully selected to balance computational efficiency and accuracy. A mesh size of 0.1 mm was used, corresponding to 10 elements per mm. The total numbers of FEM nodes and elements were approximately 1,000,000 and 700,000, respectively. A Cartesian mesh with a projection factor of 0.5 was applied to ensure high accuracy while avoiding mesh failures that can result from excessive projection factors. This modeling approach allowed for accurate thermal profiling at the lattice nodes and struts, providing critical insights into temperature differentials and their influence on the material's microstructure. Temperature-dependent thermal data, including density, thermal conductivity, and heat capacity of 316 L stainless steel, used for the simulations, are provided in Fig. 2.

## 3. Results and discussion

### 3.1. Transient thermal analysis to determine local thermal history at the node and strut

Thermal profiles at the nodes and struts of the lattice structure were

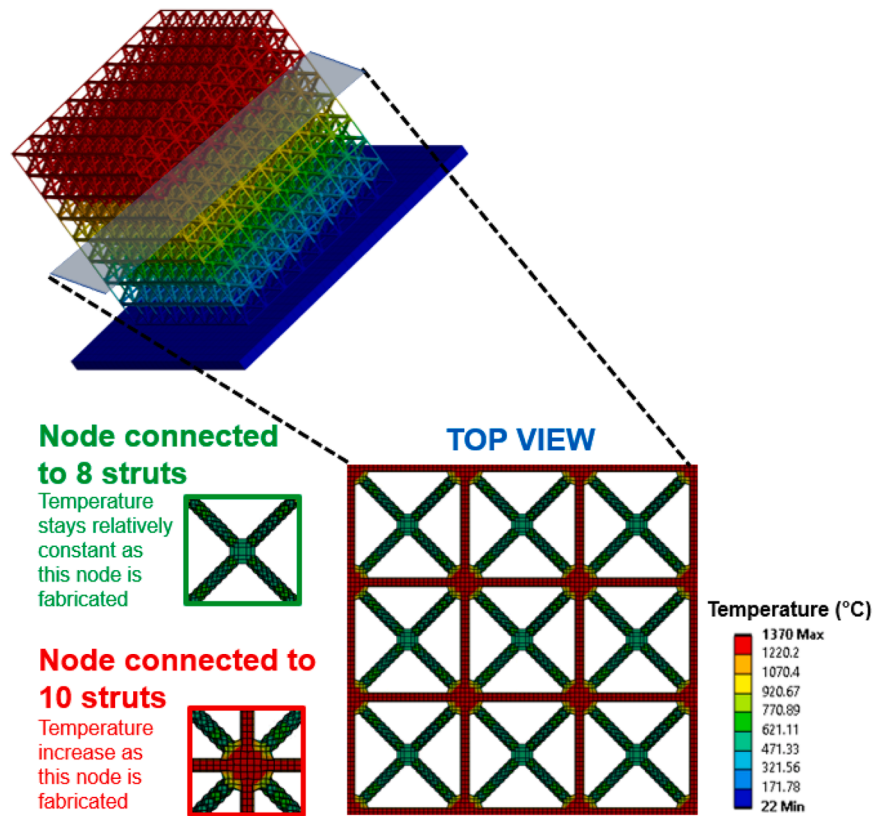


**Fig. 5.** Isometric view of the  $8 \times 8 \times 8$  FCC lattice structure and a sectioned view showing the connectivity of different types of nodes: connected by 6 struts and connected by 10 struts. Both types exhibit different thermal profiles, as shown in the enlarged top view from the LPBF hotspot calculation. The hotspot represents the temperature a layer cools down to before another layer is deposited.

recorded during the LPBF process. Transient thermal analysis [35] was utilized to calculate temperature variations over time, enabling a detailed mapping of the temperature distribution across the lattice during the LPBF process.

Following the analysis, temperature probes were placed at specific locations on the top, middle, and bottom of the lattice structure, as depicted in Fig. 3. These probes recorded temperature data as the laser approached and captured the effects of thermal cycling [36,37], which are crucial for understanding the microstructural evolution of the material.

As seen in Fig. 3, temperature probes were placed along the lattice geometry to determine the thermal responses. A graph plotting the temperature recorded by the probe over time, as seen in Fig. 4, shows that the temperature rises to  $1370^\circ\text{C}$  during the scanning of the node, corresponding to the local temperature when the laser scans the node. The temperature at the probe location subsequently decreases as the laser moves on to scan the latter parts of the structure. As the laser scans the subsequent part of the lattice structure, thus moving away from the probe, we see this decrease in temperature.

Over time, subsequent temperature spikes occur, although they are not nearly as strong as the initial  $1370^\circ\text{C}$  peak shown in Fig. 4. These peaks appear periodically, with each subsequent peak showing a decrease in intensity. The appearance of these peaks represents periodic temperature rises at the probe location, that is, the probe senses a rise in temperature from the fabrication procedure. The FEM simulations reveal that the periodic temperature rise corresponds to when the laser scans the node area. When subsequent nodes are fabricated, the temperature probe records a spike, in contrast, when the laser scans the struts, no significant temperature spike is observed. This temperature variation is due to the different connectivity of the nodes to the struts at each layer [38]. As shown in Fig. 5, in the first layer, all nodes are connected to a total of ten struts: eight slant struts and two horizontal

struts. However, in the second layers, the nodes are connected only to slant struts. Thus, when the laser scans the node connected to ten struts, a temperature rise in the overall system occurs according to FEM results, which is reflected in subsequent small peaks after the initial large peak in Fig. 4. The same pattern repeats in subsequent layers, resulting in an overall increase in system's temperature, as observed by the temperature spikes shown in Fig. 4.

The temperature spikes can be attributed to the higher thermal mass of the nodes. Nodes have a greater thermal mass than the struts, allowing them to retain more heat as they are scanned by the laser. However, the release of thermal energy is also evident from the nodes due to their multiple connections to the struts. It can be inferred that when nodes with more connectivity are scanned, the overall temperature of the system rises. Simulations show a temperature rise of  $100^\circ\text{C}$  in the overall lattice structure when the nodes connected to ten struts are fabricated, in comparison to the nodes which are connected to six struts the temperature rise is negligible. In relation to this, when probes are placed on the struts, their temperature also increases corresponding to when nodes are scanned. In contrast, no temperature spikes are observed when the laser scans the struts.

Fig. 6(a) represents the thermal cycling effects on the nodes and struts. Thermal cycling refers to the return of thermal energy to an already fabricated area [39]. Due to the increased connectivity of the nodes, which results in more heat transfer, the temperature at the nodes increases to a lesser extent after the initial peak compared to the struts. This is attributed to the node's connectivity, as they are linked by multiple struts, allowing heat to dissipate more efficiently into the struts. In contrast, struts, being less connected, experience a greater rise in temperature due to thermal cycling, since their heat is not as efficiently dissipated as at the nodes. Fig. 6(b) shows the cooling rates experienced by the nodes and struts. As shown, the nodes experience more severe thermal behavior compared to struts. The maximum and minimum

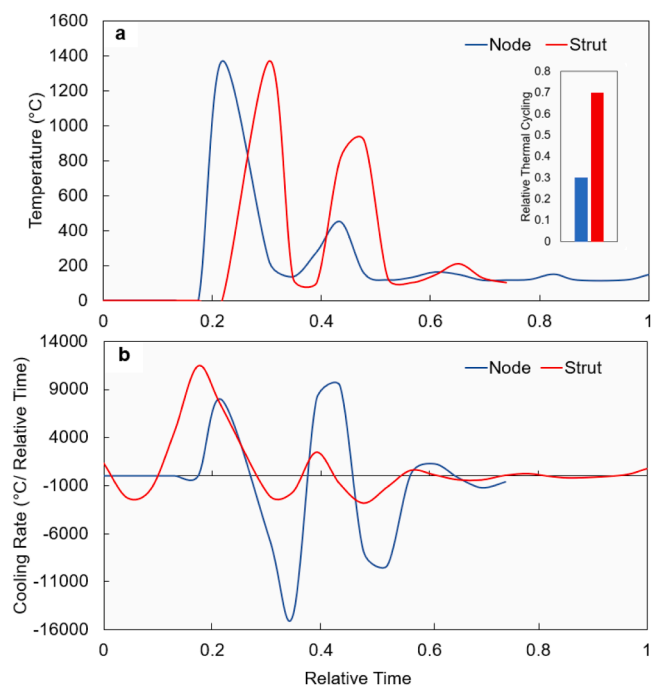


**Fig. 6.** (a) FEM simulations showing the thermal cycling effects on the nodes and struts. Nodes experience fewer cycling effects due to more heat dissipation through their increased connectivity with the struts. In contrast, struts exhibit a more pronounced thermal cycling effect than the nodes. The insert shows the relative cooling rates, implying that nodes release more thermal energy than the struts. (b) Cooling rates experienced by a particular node and strut in an FCC lattice structure, the struts experience more cooling cycles than the nodes.

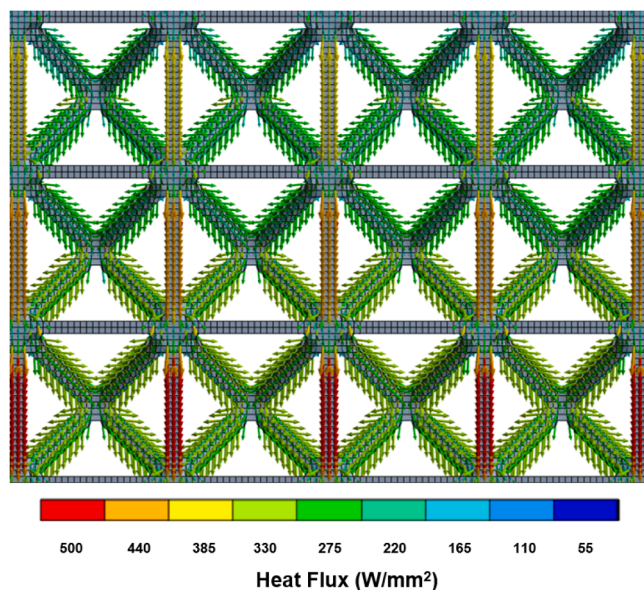


**Fig. 7.** Heat flux direction vectors obtained from FEM simulations showing the direction of heat flow from the nodes and struts of the lattice structure. Heat is dissipated in along the same gradient from the struts, as indicated by the vectors, while heat from the nodes, it is shown to dissipate outwards. The lower regions of the structure are at a higher flux (nearly 500 W/mm<sup>2</sup>) as heat is transferred from the upper region downwards as shown by the vector directions.

cooling rates of the node cover a broader range than those of the struts because the nodes accumulate more heat due to their higher thermal mass and dissipated more heat due to their connection to multiple struts.

Furthermore, FEM simulations reveal that the heat flux vectors for heat dissipation in the struts follow a single direction, as displayed in Fig. 7. The direction and magnitude of the vectors are noteworthy. The heat flux vectors show a higher magnitude for struts, this can be attributed to the geometry and continuity of the struts, which allow them to conduct heat along their direction. For nodes, the heat flux is less in magnitude as heat is dissipated and conducted to the struts joining the nodes. The direction of the vectors for struts follows the same gradient as seen in Fig. 7. For nodes, the vectors are directed out of the nodes which implies heat transfer to the adjoining struts. The area at the lower section of the struts is at a higher flux (500 W/mm<sup>2</sup>) than the upper section (250 W/mm<sup>2</sup>), implying heat is transferred from the upper side of the structure to the lower as a temperature difference of nearly 250 W/mm<sup>2</sup> is observed at both ends. The heat flux vectors are also observed to be less concentrated near the nodes, implying more heat conduction at the nodes. This heat is conducted from the nodes to the struts, which in turn leads to struts dissipating the heat conducted towards them from the node. This observation supports microstructure analysis, confirming that heat dissipation in the strut occurs in a single direction, leading to the characteristic microstructure of the struts, as observed.

### 3.2. Verification of thermal profiles through microstructural characterization and FEM simulations

This difference in thermal history between the nodes and struts directly impacts the microstructure [23], as seen in Figs. 8(a) and 9(a), specifically in terms of grain morphology. The higher thermal cycling effect in the struts, combined with their smaller cross-sectional area compared to the nodes, promotes grain orientation in a particular direction, as predicted by FEA simulations. This results in the formation of elongated grains aligned with the thermal gradients, as seen in Fig. 8(a). Rapid cooling and repeated heating encourage grain growth along the heat flow direction, contributing to the elongation of grains along the strut length [23]. Since the struts have less surrounding material to conduct heat than the nodes, they exhibit a higher level of grain elongation compared to the nodes [40–42].

As mentioned earlier, heat dissipation in the struts occurs in a specific direction, as evidenced by the microstructure in Fig. 9(a). Although nodes have a higher thermal mass than struts and can theoretically retain more heat, their increased connectivity creates a more dissipative thermal environment, reducing thermal cycling effects and resulting in a less oriented microstructure, as seen in the microstructure of the nodes. This heat dissipation changes with different geometries since there is different connectivity of node and strut in each geometry, such as FCC and BCC will exhibit different thermal behavior which in result results in microstructural changes [43,44]. A change in geometry manifests in varying mechanical properties as is shown by the studies conducted [45, 46]. Currently our study focuses on thermal properties at the node and strut with one particular diameter of the strut, studies conducted with the scope of varying strut diameters have been reported where 316 L stainless steel strut diameters were varied ranging 0.25 mm to 0.5 mm [40] with other studies focused on changing process parameters on strut diameter variation [23].

The heat dissipation behavior in the nodes occurs through a distinct mechanism compared to that in the struts, largely due to node's increased thermal connectivity with surrounding struts [47]. This connectivity facilitates more effective heat dissipation at the nodes, but the lower thermal cycling in these regions leads to less directional grain growth [48]. Unlike the struts, where higher thermal cycling and localized heating drive directional grain growth, the nodes exhibit a more isotropic thermal environment [49,50].

The higher thermal mass of the nodes reduces temperature gradients, leading to less elongated grain structures. This behavior results in more randomized grain orientation and size distribution in the node, while the struts, subjected to higher temperature gradients, promote more

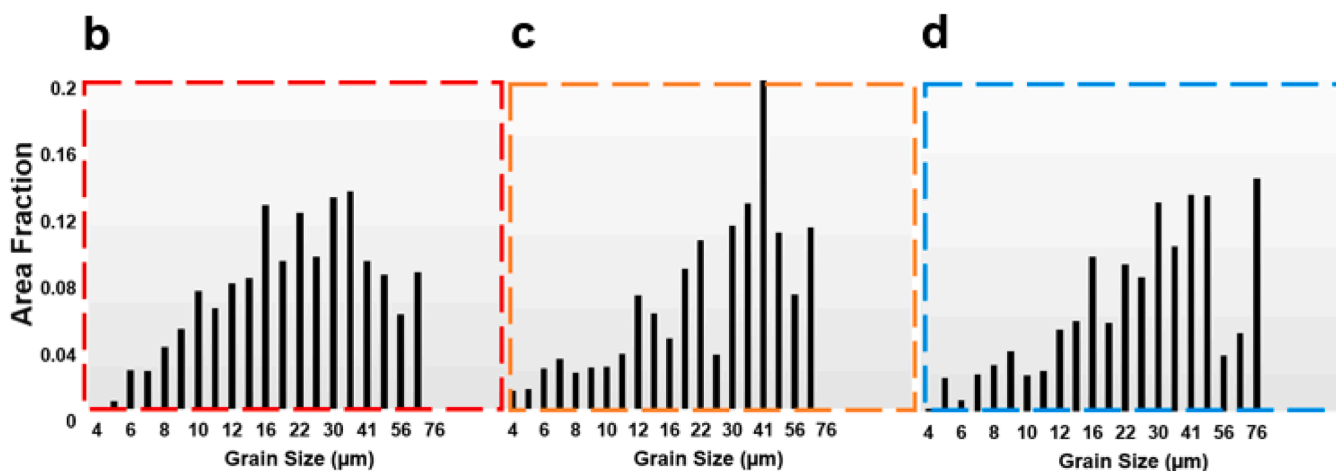
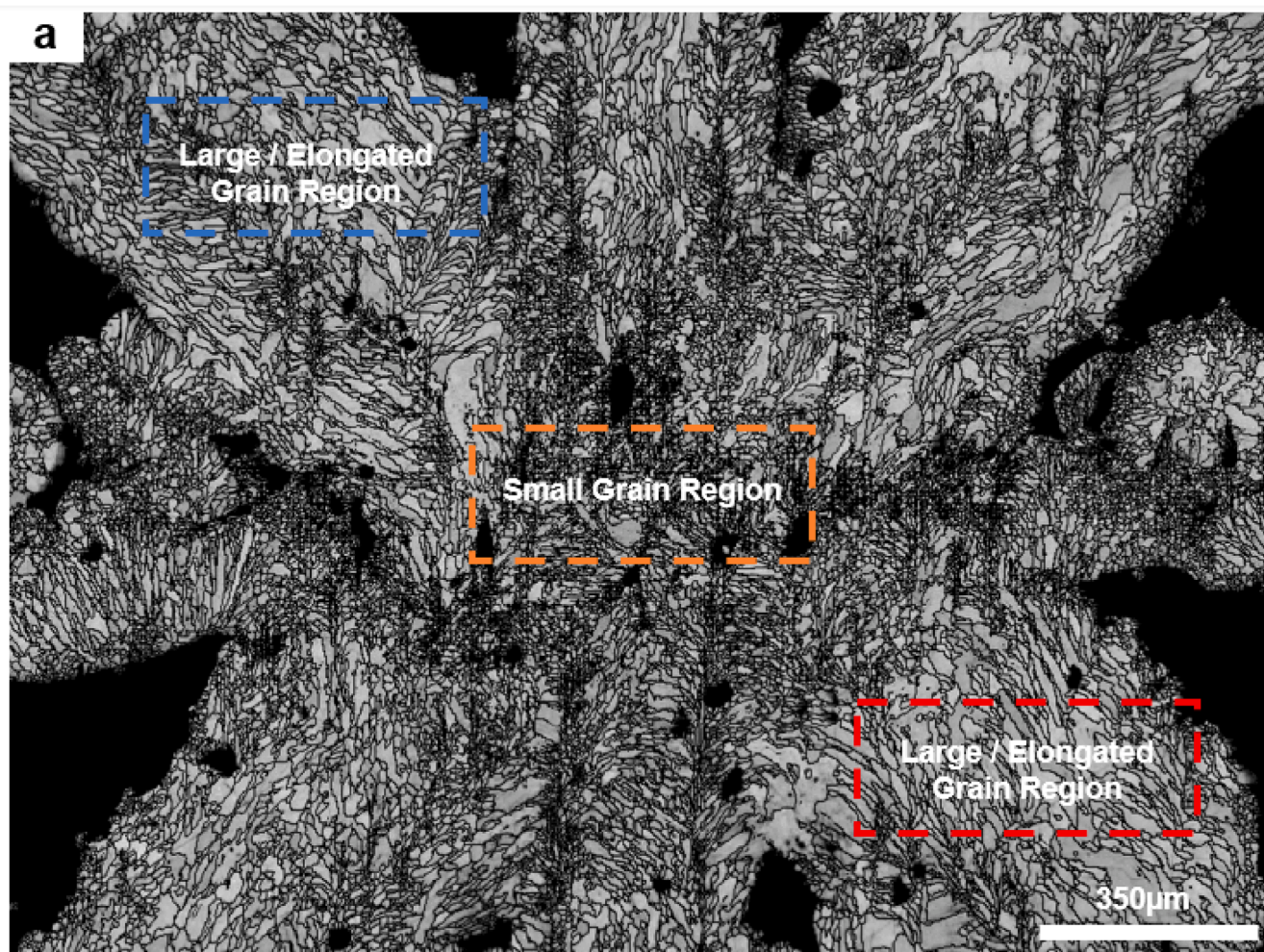


Fig. 8. (a) Grain size differences between the node and strut, the grains at the nodes are smaller in size than the ones on the strut due to thermal histories being different at each region. Average grain size graph of (c) top, (d) middle and (e) bottom nodes and struts.

elongated grains due to directional solidification [51,52]. The structural and thermal differences between the nodes and struts directly influence grain morphology. The nodes exhibit smaller and less elongated grains compared to the struts, which experience more directional solidification due to the steep temperature gradients associated with LPPF processing. Grain size analysis, as illustrated in Fig. 8(c-e), shows that the average grain size in the struts is significantly larger than in the nodes. The average grain sizes measured in the upper and lower elongated regions

( $33 \pm 20 \mu\text{m}$  and  $44 \pm 20 \mu\text{m}$ , respectively) are substantially larger than those in the small-grain regions of the nodes, which average  $26 \pm 15 \mu\text{m}$ .

This variance in grain morphology between the nodes and struts can be attributed to the accurate prediction of thermal profiles using the FEM simulations [53]. These simulations revealed that the struts experience higher peak temperatures and greater thermal cycling compared to the nodes, which are more insulated by their surrounding geometry.

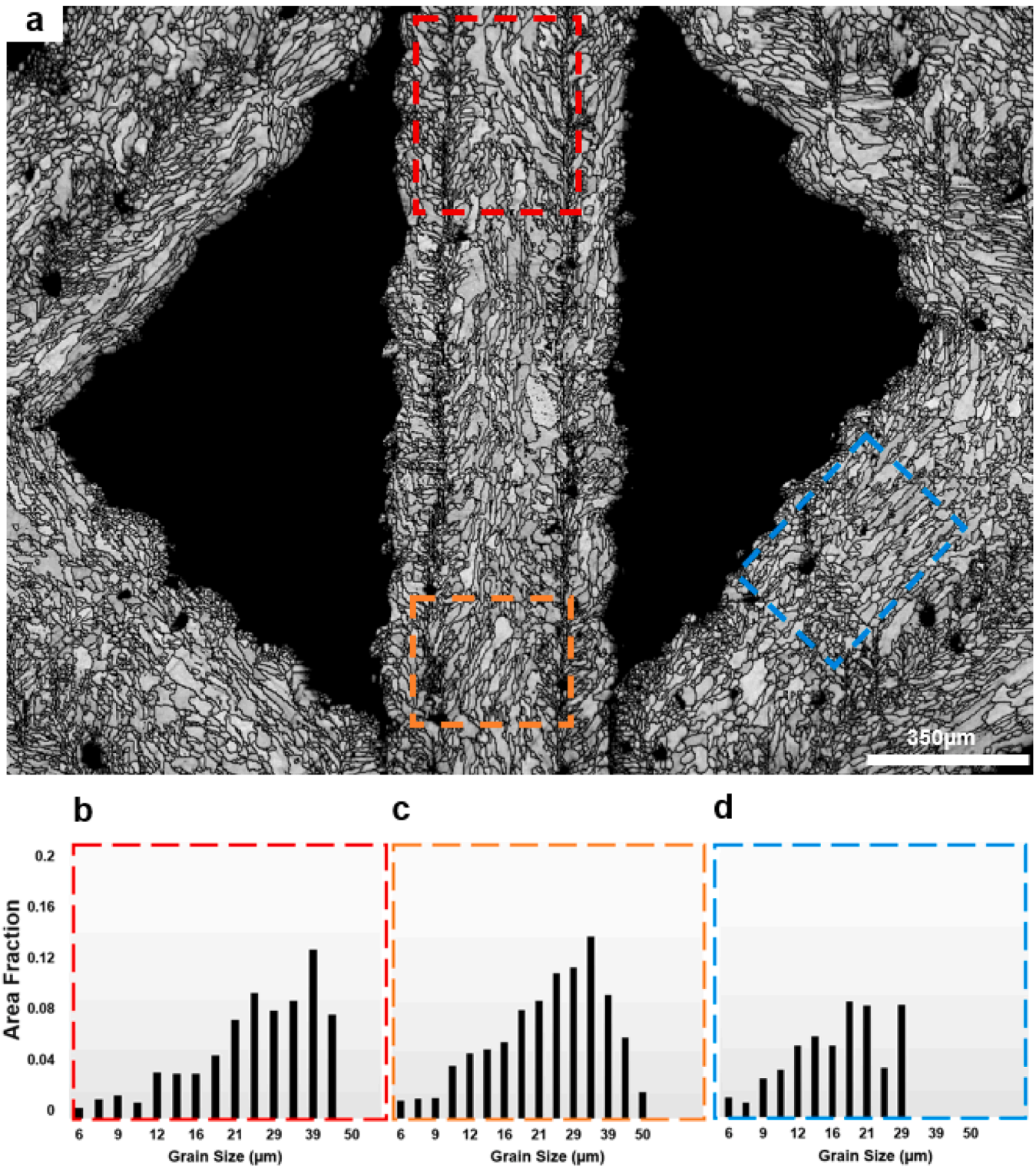


Fig. 9. (a) Grain size difference at different locations in a strut, with (b), (c), and (d) showing grain size bar graphs in the red, orange, and blue regions, respectively.

Consequently, the thermal environment of the struts promotes faster grain growth and elongation along the heat flow direction, while the nodes remain in a more thermally stable region, resulting in slower grain growth with less orientation dependence. The clear correlation between thermal profiles and the resulting grain morphology emphasizes the importance of considering local thermal conditions in the design and optimization of lattice structures for additive manufacturing processes.

The slant strut represented by the blue region, shows an average

grain size of 30 μm. However, as seen in Fig. 9(c), the slant strut contains a higher fraction of larger grains compared to the vertical strut, as highlighted in the green box. This difference can be attributed to the orientation of the slant strut, which may experience different thermal and mechanical conditions during processing, such as less severe cooling rates or thermal cycling compared to the vertical strut [54]. The relative angle of the slant strut to the heat source and the build plate could result in prolonged heat retention, allowing for grain coarsening and thus a

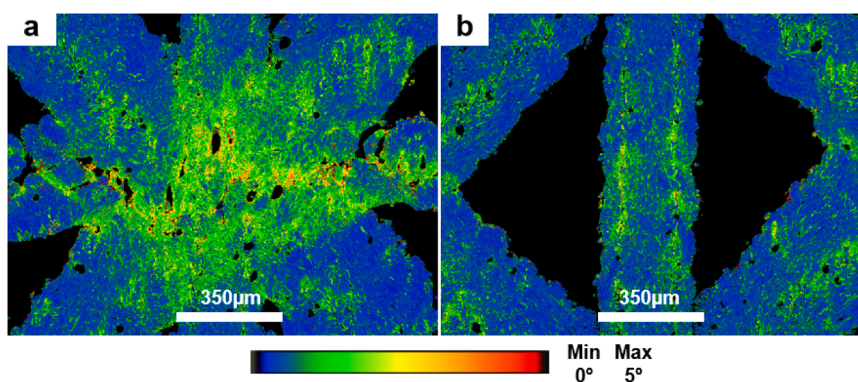


Fig. 10. KAM maps in (a) a node (b) a strut. KAM analysis shows that node regions are more distorted, attributed to rapid heat dissipation from the nodes. Cross-section area variation causes more distortion in the middle region of the strut, as seen in (b).

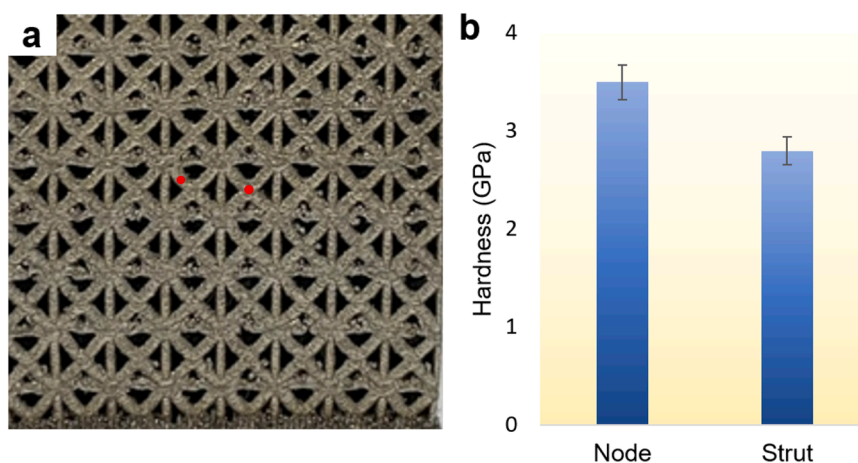


Fig. 11. (a) Sectioned FCC lattice sample showing nodes and struts (red dots) where nanoindentation hardness tests were conducted, and (b) results showing that the nodes have higher hardness values than the struts.

greater fraction of large grains.

The KAM map in Fig. 10 shows more pronounced distortion in the middle regions of the strut, which is linked to the non-uniform cross-sectional geometry in this area. This uneven cross-sectional profile likely results from the specific conditions of the LPBF process, where variations in energy input or material deposition rates can lead to a more irregular mass distribution at the middle sections of the struts [30]. The irregularities in mass and geometry contribute to stress concentrations during cooling, manifesting as increased misorientation and grain boundary distortion, as reflected in the KAM map. This higher level of distortion could influence the mechanical performance of the structure, as regions with greater misorientation may exhibit reduced ductility or increased susceptibility to localized failure under stress.

These distortions can also affect properties such as hardness, which may differ between nodes and struts as a result of their distinct thermal histories [55]. This was confirmed by nano-indentation results shown in Fig. 11 which indicate that the node regions, on average, showed higher hardness values ( $3.5 \pm 0.3$  GPa) than the struts ( $2.8 \pm 0.4$  GPa). Although the differences are minimal, the numerous indentations performed on the sample confirm the consistency of these results.

### 3.3. Porosity and variance in cross-section area of the node and strut and implications for practical use

To estimate the pore fraction in the nodes and struts, and to determine variations in cross-section areas of the struts, a total of six Optical Microscope Images (OM) were analyzed using image processing

software ImageJ. These images contained a total of 3 nodes and 18 struts. It was determined that the pore fraction of nodes was less than that of struts, confirming more thermal energy at the nodes which would result in more consolidation of mass. Further, of the two types of struts, slant and vertical struts showed less variation in cross section area. The node in Fig. 12(c) and (d) had 4 % and 6 % porosity, respectively, and the struts in Fig. 12 (g) and (h) have 8 % and 11 % fraction of pores, respectively. In addition, of the eight vertical struts examined for variation in cross section area, they exhibit less than 5 % variation in cross section area while the slant struts show almost 15 % variation in cross section area. In the sample of images taken, 10 % of struts show a major change in cross section area with more than 15 % variation.

The implications of the findings of our results have wide ranging benefits. Previous literature has reported a need for further studies of the node and strut of the lattice structure which would aim to provide more benefit to study topics such as fatigue, pores, and other processing defects resulting from thermal profiles. Indeed, the fatigue behavior of additively manufactured steel has been extensively studied and reported in literature [56–58] with studies specifically done for lattice structures [59,60] which integrate simulation studies to demonstrate that the fatigue life of steel lattices is largely influenced by processing parameters, with pores and microstructural inhomogeneities playing a critical role. Additionally, previous research has developed models to predict fatigue life [61], emphasizing that fatigue life is primarily governed by fabrication-induced defects. These studies also reveal that the fatigue strength is generally higher in the struts compared to the nodes, whereas the elastic, shear, and bulk moduli exhibit the opposite trend. Our study

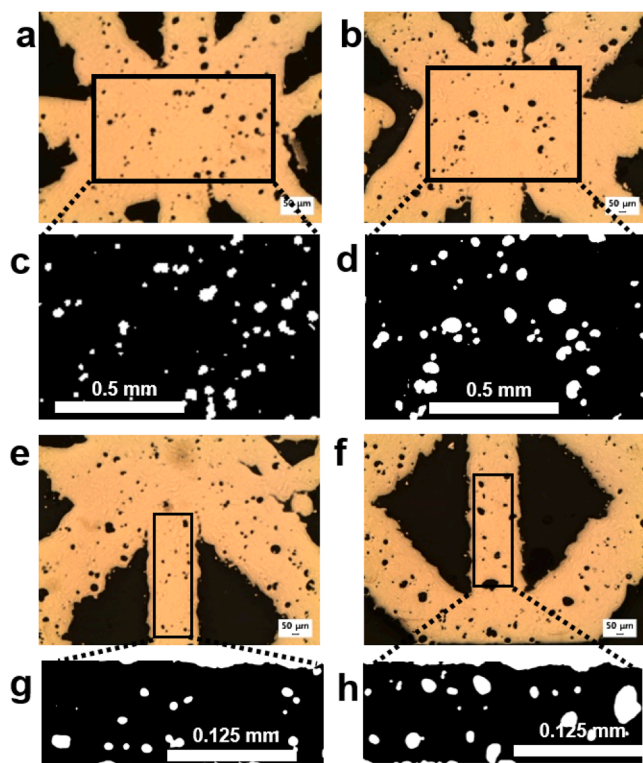


Fig. 12. OM images of the node and strut for calculating pore fraction in the node and struts and variance in cross section area of the struts (a), (b), (e), and (f) are OM images, while (c), (d), (g), and (h) are magnified images of the region on where pore fraction analysis was performed.

provides critical insights into the reasons behind these differences in mechanical properties between nodes and struts.

Building on this, other investigations have focused on the design aspects of lattice structures [62,63] aiming to develop optimized designs that offer maximum resistance to fatigue. By combining these insights with our simulation and experimental results, we contribute to a deeper understanding of the relationship between design, fabrication, and fatigue performance in lattice structures.

The insights from this study are highly relevant to the practical applications of lattice structures, as they address the powder bed fusion process and its influence on the resulting microstructure. By exploring the local thermal histories of nodes and struts, our research enhances the understanding needed for designing effective structures tailored to specific applications.

Biomedical applications, for example, demand lightweight, bio-integrative implants that mimic the properties of human bone, such as low density and high compressive strength [6]. Studies have demonstrated that lattice structures optimized through design and topology can achieve properties similar to cortical bone, making them suitable for advanced implants [64]. Moreover, research on lattice orthopedic implants highlights their functional properties, including bioactive surfaces for enhanced integration [65]. In aerospace applications, lattice structures are valued for their high strength-to-weight ratio and thermal management capabilities. Reviews emphasize the importance of processing parameters in determining product performance [66]. Given the complex geometries of lattice structures, additive manufacturing is the only viable method of production, and our focus on the thermal and microstructural behavior during processing provides a foundation for further optimization. By linking thermal behavior at the nodes and struts to the resulting microstructure, our study enables industries to design and fabricate lattices optimized for specific heat dissipation and mechanical performance.

#### 4. Conclusions

In this study, we have conducted investigations to understand the thermal behaviors of nodes and struts in 316 L stainless steel lattice structures fabricated using LPBF. This was accomplished using a combination of FEM simulations and microstructural studies. The three main conclusions are summarized as follows:

1. Thermal profiling was performed for both nodes and struts using FEM simulations. The FEM results show that the temperature of the system increases as the nodes are scanned by the laser, and more thermal cycling occurs in the struts. After reaching an initial peak temperature of 1370 °C, the nodes cooled to ~450 °C due to cycling, while the struts reach 900 °C, implying ~70 % more thermal cycling in the struts than the nodes.
2. The average grain sizes of the nodes and struts are different owing to the varying thermal histories experienced in each region. The average grain size at the nodes ( $26 \pm 15 \mu\text{m}$ ) is smaller than those at the struts ( $33 \pm 20 \mu\text{m}$  and  $44 \pm 20 \mu\text{m}$ ), reflecting the effects of localized thermal gradients.
3. The FCC lattice structures fabricated through LPBF processes demonstrate different thermal history at the nodes and struts, as confirmed by microstructural analysis. The differences in average grain size and KAM values between nodes and struts support this conclusion. Higher grain fractions (0.12) for 40  $\mu\text{m}$  sized grains were observed in the slant struts, while regions of the vertical struts showed area fractions below 0.12. The hardness values for the nodes ( $3.5 \pm 1.5 \text{ GPa}$ ) were higher than those for the struts ( $2.8 \pm 0.9 \text{ GPa}$ ). This differences in grain size and hardness confirm different local thermal histories at the nodes and struts.
4. Average porosity fraction on the node (4–6 %) is on average less than the strut (8–11 %) with vertical struts showing less variation in cross section area (5 %) than slant struts (15 %).

Currently, a few reports compare the thermal profiles of nodes and struts, making this study a foundational reference for future investigations. This study enhances the understanding of local thermal behaviors in lattice structures. Future studies will focus on structural aspect of the lattice structure, where simulations involving residual stress and deformation will be validated with experimental procedures. Studies can build up on this by developing functionally graded lattice structures using additive manufacturing techniques. By combining the insight of our results, future studies can contribute to a deeper understanding of the relationship between design fabrication and overall performance of the lattice structure.

#### CRediT authorship contribution statement

**Ahn Soung Yeoul:** Investigation. **Hashmi Muhammad Raihan:** Writing – original draft, Software, Methodology, Investigation, Formal analysis, Data curation, Conceptualization. **Jang Jae-il:** Investigation. **Lee Gitaek:** Investigation. **Wu Renhao:** Writing – review & editing, Writing – original draft, Project administration, Funding acquisition, Conceptualization. **Gao Zhe:** Investigation. **Kim Hyoung Seop:** Writing – review & editing, Supervision, Resources, Project administration, Funding acquisition, Conceptualization.

#### Declaration of Competing Interest

The authors declare that they have no known competing financial interests or personal relationships that could have appeared to influence the work reported in this paper.

#### Acknowledgments

The authors are greatly appreciated for the financial supports by the

National Research Foundation of Korea (NRF) grant funded by the Korea government (MSIP) (NRF-2021R1A2C3006662 and NRF-2022R1A5A1030054). Dr. Renhao Wu is supported by Brain Pool Program through the NRF of Korea, funded by the Ministry of Science and ICT (NRF-RS202300263999).

## Data Availability

Data will be made available on request.

## References

- [1] D. Weaire, Kelvin's foam structure: a commentary, *Philos. Mag. Lett.* 88 (2) (2008) 91–102.
- [2] D. Melancon, Z.S. Bagheri, R.B. Johnston, L. Liu, M. Tanzer, D. Pasini, Mechanical characterization of structurally porous biomaterials built via additive manufacturing: experiments, predictive models, and design maps for load-bearing bone replacement implants, *Acta Biomater.* 63 (2017) 350–368, <https://doi.org/10.1016/j.actbio.2017.09.013>.
- [3] H. Yasuda, T. Kunimine, Energy absorption of AlSi10Mg origami cellular structures fabricated via laser powder bed fusion, *MRS Commun.* 14 (4) (2024) 496–502, <https://doi.org/10.1557/s43579-024-00518-7>.
- [4] W.P. Syam, W. Jianwei, B. Zhao, I. Maskery, W. Elmadih, R. Leach, Design and analysis of strut-based lattice structures for vibration isolation, *Precis. Eng.* 52 (2018) 494–506.
- [5] H. Kurita, P. Lohmuller, P. Laheurte, K. Nakajima, F. Narita, Additive manufacturing and energy-harvesting performance of honeycomb-structured magnetostrictive Fe52–Co48 alloys, *Addit. Manuf.* 54 (2022) 102741, <https://doi.org/10.1016/j.addma.2022.102741>.
- [6] T. Maconachie, et al., SLM lattice structures: properties, performance, applications and challenges, *Mater. Des.* 183 (2019) 108137.
- [7] L.-Y. Chen, S.-X. Liang, Y. Liu, L.-C. Zhang, Additive manufacturing of metallic lattice structures: unconstrained design, accurate fabrication, fascinating performances, and challenges, *Mater. Sci. Eng.: R Rep.* 146 (2021) 100648, <https://doi.org/10.1016/j.mser.2021.100648>.
- [8] M. Zhao, X. Li, D.Z. Zhang, W. Zhai, Design, mechanical properties and optimization of lattice structures with hollow prismatic struts, *Int. J. Mech. Sci.* 238 (2023) 107842, <https://doi.org/10.1016/j.ijmecsci.2022.107842>.
- [9] C. Li, et al., Architecture design of periodic truss-lattice cells for additive manufacturing, *Addit. Manuf.* 34 (2020) 101172.
- [10] C. Yan, L. Hao, A. Hussein, P. Young, D. Raymont, Advanced lightweight 316L stainless steel cellular lattice structures fabricated via selective laser melting, *Mater. Des.* 55 (2014) 533–541, <https://doi.org/10.1016/j.matdes.2013.10.027>.
- [11] F. Caiazzo, V. Alfieri, S.L. Campanelli, V. Errico, Additive manufacturing and mechanical testing of functionally-graded steel strut-based lattice structures, *J. Manuf. Process.* 83 (2022) 717–728, <https://doi.org/10.1016/j.jmapro.2022.09.031>.
- [12] J. Wei, J. Wang, J. Yang, Y. Zeng, Y. Guan, Effect of internal defects on the compression behavior of stainless steel lattice structure fabricated by selective laser melting, *J. Manuf. Process.* 120 (2024) 809–826, <https://doi.org/10.1016/j.jmapro.2024.04.049>.
- [13] N.S. Johnson, et al., Direct measurement of the effective properties of an additively manufactured titanium octet truss unit cell using high energy X-ray diffraction, *Mater. Charact.* 209 (2024) 113755.
- [14] A. Bertocco, G. Iannitti, A. Caraviello, L. Esposito, Lattice structures in stainless steel 17-4PH manufactured via selective laser melting (SLM) process: dimensional accuracy, satellites formation, compressive response and printing parameters optimization, *Int. J. Adv. Manuf. Technol.* 120 (7) (2022) 4935–4949, <https://doi.org/10.1007/s00170-022-08946-2>.
- [15] F. Veloso, J. Gomes-Fonseca, P. Morais, J. Correia-Pinto, A.C.M. Pinho, J.L. Vilaça, Overview of methods and software for the design of functionally graded lattice structures, *Adv. Eng. Mater.* 24 (11) (2022) 2200483, <https://doi.org/10.1002/adem.202200483>.
- [16] A.T. Erturk, M.E. Bulduk, G. Tarakçi, G. Özer, E. Yazar, Investigation of the microstructure and mechanical characteristics of lattice structures produced by laser powder bed fusion method, *Met. Mater. Int.* 28 (1) (2022) 155–167, <https://doi.org/10.1007/s12540-021-01038-y>.
- [17] K. Kappe, K. Hoschke, W. Riedel, S. Hiermaier, Multi-objective optimization of additive manufactured functionally graded lattice structures under impact, *Int. J. Impact Eng.* 183 (2024) 104789, <https://doi.org/10.1016/j.ijimpeng.2023.104789>.
- [18] P. Terriault, V. Brailovski, Modeling and simulation of large, conformal, porosity-graded and lightweight lattice structures made by additive manufacturing, *Finite Elem. Anal. Des.* 138 (2018) 1–11, <https://doi.org/10.1016/j.finel.2017.09.005>.
- [19] Y. Chen, Q. Li, X. Chen, J. Tan, H. He, Coupled CA-FE simulation for dynamic recrystallization microstructure evolution of AZ61 magnesium alloy, *Met. Mater. Int.* (2024), <https://doi.org/10.1007/s12540-024-01757-y>.
- [20] Q. Xu, X. Yang, J. Liu, Z. Qiu, G. Li, Reconstruction mechanism of surface integrity for laser additive manufactured 316 L stainless steel subjected to ultrasonic surface rolling process: numerical simulation and experimental verification, *Met. Mater. Int.* (2024), <https://doi.org/10.1007/s12540-024-01683-z>.
- [21] G. Chen, et al., Efficient reduced-order thermal modelling of scanning laser melting for additive manufacturing, *J. Mater. Process. Technol.* 321 (2023) 118163, <https://doi.org/10.1016/j.jmatprotec.2023.118163>.
- [22] J. Ding et al., Imperfection-Enabled Strengthening of Ultra-Lightweight Lattice Materials, *Advanced Science*, vol. n/a, no. n/a, p. 2402727, <https://doi.org/10.1002/adv.202402727>.
- [23] C. Britt, C.J. Montgomery, M.J. Brand, Z.-K. Liu, J.S. Carpenter, A.M. Beese, Effect of processing parameters and strut dimensions on the microstructures and hardness of stainless steel 316L lattice-emulating structures made by powder bed fusion, *Addit. Manuf.* 40 (2021) 101943.
- [24] Z. Yang, J.A. Koepf, M. Markl, C. Körner, Effect of scanning strategies on grain structure and texture of additively manufactured lattice struts: a numerical exploration, *Adv. Eng. Mater.* (2024) 2400661.
- [25] Z. Gao, et al., Damage-programmable design of metamaterials achieving crack-resisting mechanisms seen in nature, *Nat. Commun.* 15 (1) (2024) 7373, <https://doi.org/10.1038/s41467-024-51757-0>.
- [26] M. Liu, N. Takata, A. Suzuki, M. Kobashi, Development of gradient microstructure in the lattice structure of AlSi10Mg alloy fabricated by selective laser melting, *J. Mater. Sci. Technol.* 36 (2020) 106–117, <https://doi.org/10.1016/j.jmst.2019.06.015>.
- [27] Y. Estrin, Y. Beygelzimer, R. Kulagin, Design of architected materials based on mechanically driven structural and compositional patterning, *Adv. Eng. Mater.* 21 (9) (2019) 1900487, <https://doi.org/10.1002/adem.201900487>.
- [28] Y. Estrin, V.R. Krishnamurthy, E. Akleman, Design of architected materials based on topological and geometrical interlocking, *J. Mater. Res. Technol.* 15 (2021) 1165–1178, <https://doi.org/10.1016/j.jmrt.2021.08.064>.
- [29] R. Kulagin, Y. Beygelzimer, A. Bachmaier, R. Pippan, Y. Estrin, Benefits of pattern formation by severe plastic deformation, *Appl. Mater. Today* 15 (2019) 236–241, <https://doi.org/10.1016/j.apmt.2019.02.007>.
- [30] M. Alaña, A. Cutolo, G. Probst, S. Ruiz de Galarreta, B. Van Hooreweder, Understanding elastic anisotropy in diamond based lattice structures produced by laser powder bed fusion: Effect of manufacturing deviations, *Mater. Des.* 195 (2020) 108971, <https://doi.org/10.1016/j.matdes.2020.108971>.
- [31] X. Sheng, et al., Laser powder bed fusion for the fabrication of triply periodic minimal surface lattice structures: synergistic macroscopic and microscopic optimization, *J. Manuf. Process.* 119 (2024) 179–192.
- [32] M.F. Ashby, *Metal Foams: A Design Guide*, Elsevier, 2000.
- [33] G. Lee, et al., Shear deformation behavior of additively manufactured 316L stainless steel lattice structures, *Addit. Manuf.* 93 (2024) 104425, <https://doi.org/10.1016/j.addma.2024.104425>.
- [34] Y. Xiao, et al., A gleeble-assisted study of phase evolution of Ti-6Al-4V induced by thermal cycles during additive manufacturing, *J. Alloy. Compd.* 860 (2021) 158409, <https://doi.org/10.1016/j.jallcom.2020.158409>.
- [35] K. Deshmukh, et al., Effect of processing parameters and thermal history on microstructure evolution and functional properties in laser powder bed fusion of 316L, *Mater. Des.* 244 (2024) 113136, <https://doi.org/10.1016/j.matdes.2024.113136>.
- [36] L. Palmeira Belotti, J.A.W. van Dommelen, M.G.D. Geers, C. Goulas, W. Ya, J.P. M. Hoefnagels, Microstructural characterisation of thick-walled wire arc additively manufactured stainless steel, *J. Mater. Process. Technol.* 299 (2022) 117373, <https://doi.org/10.1016/j.jmatprotec.2021.117373>.
- [37] C. Jiang, W. Hao, C. Liu, D. Shi, W. Song, Thermal cycling performance of GYbZ/YSZ thermal barrier coatings with different microstructures based on finite element simulation, *J. Alloy. Compd.* 1010 (2025) 177185, <https://doi.org/10.1016/j.jallcom.2024.177185>.
- [38] S. Kechagias, R.N. Oosterbeek, M.J. Munford, S. Ghouse, J.R.T. Jeffers, Controlling the mechanical behaviour of stochastic lattice structures: the key role of nodal connectivity, *Addit. Manuf.* 54 (2022) 102730, <https://doi.org/10.1016/j.addma.2022.102730>.
- [39] H. Chae, et al., Unravelling thermal history during additive manufacturing of martensitic stainless steel, *J. Alloy. Compd.* 857 (2021) 157555, <https://doi.org/10.1016/j.jallcom.2020.157555>.
- [40] X. Wang, J.A. Muñoz-Lerma, O. Sánchez-Mata, M. Attarian Shandiz, M. Brochu, Microstructure and mechanical properties of stainless steel 316L vertical struts manufactured by laser powder bed fusion process, *Mater. Sci. Eng.: A* 736 (2018) 27–40, <https://doi.org/10.1016/j.msea.2018.08.069>.
- [41] Z. Dong, et al., Revealing anisotropic mechanisms in mechanical and degradation properties of zinc fabricated by laser powder bed fusion additive manufacturing, *J. Mater. Sci. Technol.* 214 (2025) 87–104, <https://doi.org/10.1016/j.jmst.2024.06.045>.
- [42] J.K. Tiwari, V.K. Singh, T. Anwer, M. Ashiq, M. Amirthalingam, Investigation of microstructure and thermal expansion behaviour of a functionally graded YSZ/IN718 composite produced by laser-powder bed fusion, *J. Alloy. Compd.* 1005 (2024) 175947, <https://doi.org/10.1016/j.jallcom.2024.175947>.
- [43] M. Sos, G. Meyer, K. Durst, C. Mittelstedt, E. Bruder, Microstructure and mechanical properties of additively manufactured AlSi10Mg lattice structures from single contour exposure, *Mater. Des.* 227 (2023) 111796.
- [44] J. Yang, W. Li, Comparative study on the process, anisotropy, and mechanical performance of laser powder bed fusion fabricated truss-lattice structures with different unit cell designs, *CIRP J. Manuf. Sci. Technol.* 52 (2024) 307–317.
- [45] J. Niu, H.L. Choo, W. Sun, S.H. Mok, Numerical study on load-bearing capabilities of beam-like lattice structures with three different unit cells, *Int. J. Mech. Mater. Des.* 14 (3) (2018) 443–460, <https://doi.org/10.1007/s10999-017-9384-3>.
- [46] N. Qiu, Y. Wan, Y. Shen, J. Fang, Experimental and numerical studies on mechanical properties of TPMS structures, *Int. J. Mech. Sci.* 261 (2024) 108657, <https://doi.org/10.1016/j.ijmecsci.2023.108657>.

- [47] Z. Zhang, et al., Bioinspired, simulation-guided design of polyhedron metamaterial for simultaneously efficient heat dissipation and energy absorption, *Adv. Mater. Technol.* 7 (10) (2022) 2200076, <https://doi.org/10.1002/admt.202200076>.
- [48] M.J. SaGong, et al., Repairability and effectiveness in direct energy deposition of 316L stainless steel grooves: a comparative study on varying laser strategy, *J. Mater. Res. Technol.* 32 (2024) 3347–3356, <https://doi.org/10.1016/j.jmrt.2024.08.181>.
- [49] S.J. Sun, Y.Z. Tian, H.R. Lin, Z.J. Wang, Z.F. Zhang, Revisiting the role of prestrain history in the mechanical properties of ultrafine-grained CoCrFeMnNi high-entropy alloy, *Mater. Sci. Eng.: A* 801 (2021) 140398, <https://doi.org/10.1016/j.msea.2020.140398>.
- [50] L. Lemarquis, P.F. Giroux, H. Maskrot, B. Barkia, O. Hercher, P. Castany, Cold-rolling effects on the microstructure properties of 316L stainless steel parts produced by Laser Powder Bed Fusion (LPBF), *J. Mater. Res. Technol.* 15 (2021) 4725–4736, <https://doi.org/10.1016/j.jmrt.2021.10.077>.
- [51] H. Liu, et al., Dimensional effect and mechanical performance of node-strengthened hybrid lattice structure fabricated by laser powder bed fusion, *Virtual Phys. Prototyp.* 18 (1) (2023) e2240306, <https://doi.org/10.1080/17452759.2023.2240306>.
- [52] S. Roos, C. Botero, J. Danvind, A. Koptioug, L.-E. Rännar, Macro- and micromechanical behavior of 316LN lattice structures manufactured by electron beam melting, *J. Mater. Eng. Perform.* 28 (12) (2019) 7290–7301, <https://doi.org/10.1007/s11665-019-04484-3>.
- [53] M. Jalali, et al., SLM additive manufacturing of NiTi porous implants: a review of constitutive models, finite element simulations, manufacturing, heat treatment, mechanical, and biomedical studies, *Met. Mater. Int.* 29 (9) (2023) 2458–2491, <https://doi.org/10.1007/s12540-023-01401-1>.
- [54] M.J. SaGong, et al., Enhanced strength-ductility synergy in stainless steel 316L through hierarchically tailored microstructure via laser-based repair deposition, *Mater. Res. Lett.* 12 (10) (2024) 709–718, <https://doi.org/10.1080/21663831.2024.2378732>.
- [55] H.M. Joo, et al., Effect of cell geometry and heat treatment on the energy absorption property of AlSi10Mg alloy lattice structures produced by laser-based powder bed fusion, *Met. Mater. Int.* 30 (5) (2024) 1294–1306, <https://doi.org/10.1007/s12540-023-01567-8>.
- [56] P. Kumar, R. Jayaraj, J. Suryawanshi, U.R. Satwik, J. McKinnell, U. Ramamurty, Fatigue strength of additively manufactured 316L austenitic stainless steel, *Acta Mater.* 199 (2020) 225–239, <https://doi.org/10.1016/j.actamat.2020.08.033>.
- [57] K. Solberg, S. Guan, N. Razavi, T. Welo, K.C. Chan, F. Berto, Fatigue of additively manufactured 316L stainless steel: the influence of porosity and surface roughness, *Fatigue Fract. Eng. Mater. Struct.* 42 (9) (2019) 2043–2052, <https://doi.org/10.1111/ffe.13077>.
- [58] S. Lee, J.W. Pegues, N. Shamsaei, Fatigue behavior and modeling for additive manufactured 304L stainless steel: the effect of surface roughness, *Int. J. Fatigue* 141 (2020) 105856, <https://doi.org/10.1016/j.ijfatigue.2020.105856>.
- [59] P. Köhnen, C. Haase, J. Bültmann, S. Ziegler, J.H. Schleifenbaum, W. Bleck, Mechanical properties and deformation behavior of additively manufactured lattice structures of stainless steel, *Mater. Des.* 145 (2018) 205–217, <https://doi.org/10.1016/j.matdes.2018.02.062>.
- [60] G. Alaimo, M. Carraturo, N. Korshunova, S. Kollmannsberger, Numerical evaluation of high cycle fatigue life for additively manufactured stainless steel 316L lattice structures: preliminary considerations, *Mater. Des. Process. Commun.* 3 (4) (2021), <https://doi.org/10.1002/mdp2.249>.
- [61] A. Burr, et al., A numerical framework to predict the fatigue life of lattice structures built by additive manufacturing, *Int. J. Fatigue* 139 (2020) 105769, <https://doi.org/10.1016/j.ijfatigue.2020.105769>.
- [62] E. Masoumi Khalil Abad, S. Arabnejad Khanoki, D. Pasini, Fatigue design of lattice materials via computational mechanics: application to lattices with smooth transitions in cell geometry, *Int. J. Fatigue* 47 (2013) 126–136, <https://doi.org/10.1016/j.ijfatigue.2012.08.003>.
- [63] L. Boniotti, S. Beretta, L. Patriarca, L. Rigoni, S. Foletti, Experimental and numerical investigation on compressive fatigue strength of lattice structures of AlSi7Mg manufactured by SLM, *Int. J. Fatigue* 128 (2019) 105181, <https://doi.org/10.1016/j.ijfatigue.2019.06.041>.
- [64] A.M. Vilardell, et al., Topology optimization and characterization of Ti6Al4V ELI cellular lattice structures by laser powder bed fusion for biomedical applications, *Mater. Sci. Eng.: A* 766 (2019) 138330, <https://doi.org/10.1016/j.msea.2019.138330>.
- [65] X.Z. Zhang, M. Leary, H.P. Tang, T. Song, M. Qian, Selective electron beam manufactured Ti-6Al-4V lattice structures for orthopedic implant applications: current status and outstanding challenges, *Curr. Opin. Solid State Mater. Sci.* 22 (3) (2018) 75–99, <https://doi.org/10.1016/j.cossms.2018.05.002>.
- [66] N. Khan, A. Riccio, A systematic review of design for additive manufacturing of aerospace lattice structures: current trends and future directions, *Prog. Aerosp. Sci.* 149 (2024) 101021, <https://doi.org/10.1016/j.paerosci.2024.101021>.